Supporting Information

Low-Crystallinity Polymer Donor Enables High-Efficiency Semitransparent Organic Solar Cells under Substantial Donor Dilution

Qihang Liu, [†a] Hongxiang Li, [†b,d] Yixun Shu, [c] Zhengdong Wei, [a] Yahui Liu, [c] Pei Cheng,[d] Hao Lu, [*a] Yifan Wang, [*a] and Zhishan Bo [*c]

[a] College of Materials Science and Engineering, Qingdao University, Qingdao 266071, China

[b] College of Materials and Energy, Guang'an Institute of Technology, Guang'an 638000, China

[c] College of Textiles & Clothing, State Key Laboratory of Bio-fibers and Eco-textiles, Qingdao University, Qingdao 266071, China

[d] College of Polymer Science and Engineering, National Key Laboratory of Advanced Polymer Materials, Sichuan University, Chengdu 610065, China

[†] These authors contributed equally to this work.

[*]Corresponding author. Email: luhao@qdu.edu.cn (H. L.); wangyifan@qdu.edu.cn (Y. W.); zsbo@bnu.edu.cn (Z. B.)

Materials

All reagents and chemicals were purchased from commercial sources and were used without further purification unless noted otherwise. The photo-active materials D18[1], PL2[2], L8-BO[3], and PDINN[4] were all synthesized in according to previous literature. PM6 were purchased from Solarmer Material Inc. All solvents were purchased from Sigma-Aldrich. PEDOT:PSS (AI 4083) was sourced from Heraeus Inc.

Experimental section

Device Fabrication and Characterization

Opaque Device Fabrication: A conventional structure of ITO/PEDOT:PSS/active layer/ PDINN/Ag was used to fabricate the OSC devices. The ITO glass was first cleaned by sonicating in deionized water, acetone, and isopropanol for 20 min each. The cleaned ITO glasses were treated by UV-ozone for 40 mins. The PEDOT:PSS solution (AI 4083) was spin-coated on the ITO substrate at 5000 rpm for 25 s after 30 min, then substrates were treated by thermal annealing at 150 °C for 10 min in ambient atmosphere. All active layers were spin-coated on the PEDOT:PSS via spin-coating. The active layer solutions of D18:L8-BO, PM6:L8-BO, and PL2:L8-BO were prepared at D:A weight ratios of 1:1.2 to 1:5 using chloroform as the solvent, with DIB added as an additive. After complete dissolution, the organic layers were spin-coated onto PEDOT:PSS films and annealed at 100 °C for 1 min. Each device condition underwent systematic optimization, including active layer thickness, thermal annealing conditions, and the use of solvent additives. Subsequently, a 1.5 mg mL^{-1} solution of PIDNN was spin-coated onto the active layer at 3000 rpm for 30 s. Finally, about 100 nm Ag was evaporated onto the active layer under high vacuum (below 1×10^{-6} Torr), respectively. The effective area of a single cell is 0.04 cm^2.

Semitransparent Device Fabrication: For the PL2:L8-BO device with a D:A weight ratio of 1:4, a transparent electrode consisting of 1 nm Au and 15 nm Ag was thermally evaporated onto the PDINN layer under a high vacuum of 3×10^{-4} Pa. To further improve the ST OSCs, a MoO_3 layer (35 nm) was deposited on the Ag electrode under a pressure of 1×10^{-6} Pa.

J-V and EQE characterization: The *J-V* curves were recorded in a glove box at approximately 25℃ using an instrument from Enli Technology Ltd, Taiwan (SS-F53A) under AM 1.5G illumination (AAA class solar simulator, with an intensity of 100 mW cm^{-2} calibrated with a standard single crystal Si photovoltaic cell). External quantum efficiency (EQE) measurements were conducted in air without encapsulation. The EQE data were obtained using a solar cell spectral response measurement system (QER3011,

Enli Technology Co. Ltd), and the intensity was calibrated with a standard single crystal Si photovoltaic cell.

Photocurrent density (J_{ph}) versus effective voltage (V_{eff}) measurements: Photocurrent density (J_{ph}) versus effective voltage (V_{eff}) measurements were conducted with a comprehensive analysis based on the current density-voltage curves (voltage ranging from -2 to 2 V) obtained under both light and dark conditions. J_L is the light current density under the illumination of AM 1.5G, 100 mW cm^{-2} and J_D is the dark current density. $J_{ph} = J_L - J_D$, V_0 is the voltage when $J_L = J_D$, and V_{appl} refers to the applied voltage. $V_{eff} = V_0 - V_{appl}$. Saturation current (J_{sat}) refers to the situation when free charges in the film are totally thrusted out and collected by electrodes at a high V_{eff}.

Light-intensity dependence measurements: Light-intensity dependence measurements were conducted in a N_2-filled glove box under AM 1.5G with light intensity ranging from 10 to 100 mW cm^{-2}. The illumination was calibrated with a standard silicon solar cell equipped with a KG5 filter, certified by the National Institute of Metrology. A Keithley 2450 source-measure unit was utilized for data acquisition and control during the experiments.

Characterization: The temperature-dependent absorption (TD-Abs) spectra and UV-visible absorption spectra were obtained using a PerkinElmer UV-Vis spectrometer, model Lambda 750. Thermogravimetric analysis (TGA) was performed using a Mettler thermogravimetric analyzer (Switzerland) under nitrogen atmosphere at a heating rate of 10 °C/min with a gas flow rate of 10 ml/min over a temperature range of 30-600 °C. Atomic force microscopy (AFM) images were captured with a Multimode 8 (Bruker) in tapping mode. The in-situ absorption spectra were acquired using a halogen lamp light source on the Shanxi Puguang Vision DU-200 spectrophotometer system. The steady-state photoluminescent spectra were all recorded on the Steady/Transient State Fluorescence Spectrometer (Nano Log, Horriba Instruments).

GIWAXS Data Processing: GIWAXS data were obtained at beamline BL02U2 of Shanghai Synchrotron Radiation Facility (SSRF). The monochromatic of the light

source was 1.24 Å. The data were recorded by using the two-dimensional image plate detector of Pilatus 2M from Dectris, Switzerland. To extract the crystalline coherence length (CCL) and d-spacing, the following analysis procedure was employed: (1) Background Subtraction**:** Prior to peak fitting, a polynomial background was subtracted from the one-dimensional profiles to eliminate the diffuse scattering contributions from amorphous regions and the substrate. (2) Peak Fitting: The target diffraction peaks were fitted using a Gaussian function to determine their positions and full width at half maximum (FWHM). (3) CCL Calculation and Uncertainty Estimation: Based on the fitted FWHM, the CCL was calculated using the Scherrer equation: $CCL = \frac{2\pi k}{FWHM}$, where K is the Scherrer constant, taken as 0.9. The d-spacing of molecular stacking are calculated by the equation: $d = \frac{2\pi}{q}$

Contact angle measurements: The surface tension value ($\gamma_{SV} = \gamma_S^d + \gamma_S^P$) can be estimated from the contact angle (θ) according to the Owens-Wendt-Kaelble model[5], $\gamma_{LV}(1 + \cos\theta) = 2\left(\sqrt{\gamma_S^P \gamma_L^P} + \sqrt{\gamma_S^d \gamma_L^d}\right)$, where γ_{LV} is the surface tension of the liquid in equilibrium with its vapor and γ_{SV} is that of the solid. The degree of molecular miscibility can be evaluated by Flory-Huggins interaction parameter χ, which can be calculated by the formula:[6] $\chi_{A:B} = K\left(\sqrt{\gamma_A} - \sqrt{\gamma_B}\right)_2$

SCLC Measurements： Devices with the architecture of ITO/PEDOT:PSS/Active Layer/MoO_3/Ag and ITO/ZnO/Active Layer/PDINN/Ag were applied to construct the hole-only and electron-only device, respectively. The active layers were prepared under the optimized conditions. According to the Mott-Gurney equation:

$$J = \frac{9}{8}\varepsilon\varepsilon_0\mu\frac{V^2}{L^3}$$

Here, *J* is the current density; ε is the dielectric constant of the blend film; ε_0 is the permittivity of the vacuum; μ is the mobility; *L* is the thickness of the film; *V* is the applied voltage.

Calculation of the average visible transmittance (AVT)： The AVT value was calculated according to the average value of transmittance of semitransparent devices based on photonic response of the human eye, it characterizes the optical transparency of the device under visual inspection. The wavelength range is usually adopted by 380-780 nm, calculation formula is

$$AVT = \frac{\int T(\lambda)P(\lambda)E(\lambda)d\lambda}{\int P(\lambda)E(\lambda)d\lambda}$$

Where $T(\lambda)$ is the wavelength-dependent transmittance of the devices, $P(\lambda)$ is the spectral irradiance of AM 1.5G standard solar illumination, $E(\lambda)$ is the photonic response of the human eye.

Calculation of the color coordinates*:* The color coordinates (x, y, z) of semitransparent devices were calculated according to the transmission spectra based on chromaticity diagram of the CIE 1931xy. The color coordinates were calculated by the formulas:

$$\begin{cases} X = \int_{380}^{780} F(\lambda)T(\lambda)\bar{x}(\lambda)d\lambda \\ Y = \int_{380}^{780} F(\lambda)T(\lambda)\bar{y}(\lambda)d\lambda \\ Z = \int_{380}^{780} F(\lambda)T(\lambda)\bar{z}(\lambda)d\lambda \end{cases}$$

$$\begin{cases} x = \frac{X}{X+Y+Z} \\ y = \frac{Y}{X+Y+Z} \end{cases}$$

where X, Y, Z are tristimulus values, where F(λ) is the AM1.5G irradiation, T(λ) is the

transmission spectra, $\bar{x}(\lambda)$, $\bar{y}(\lambda)$and $\bar{z}(\lambda)$ are thecolor matching functions specified by the International Commission on Illumination.

Calculation of the CRI*:* The CRI quantitatively expresses the degree of color appearances to the real objects with values of CRI ranging from 0 to 100. It was calculated by the CIE 1931xy chromaticity diagram.

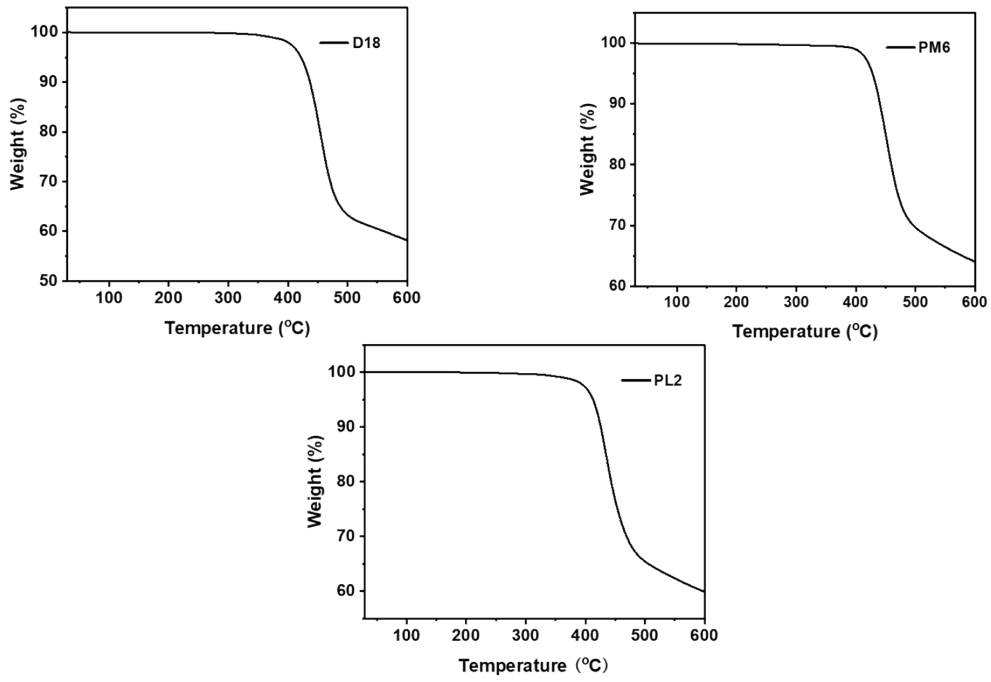

Figure S1. TGA curves of D18, PM6, and PL2 under nitrogen atmosphere at a heating rate of 10 °C/min.

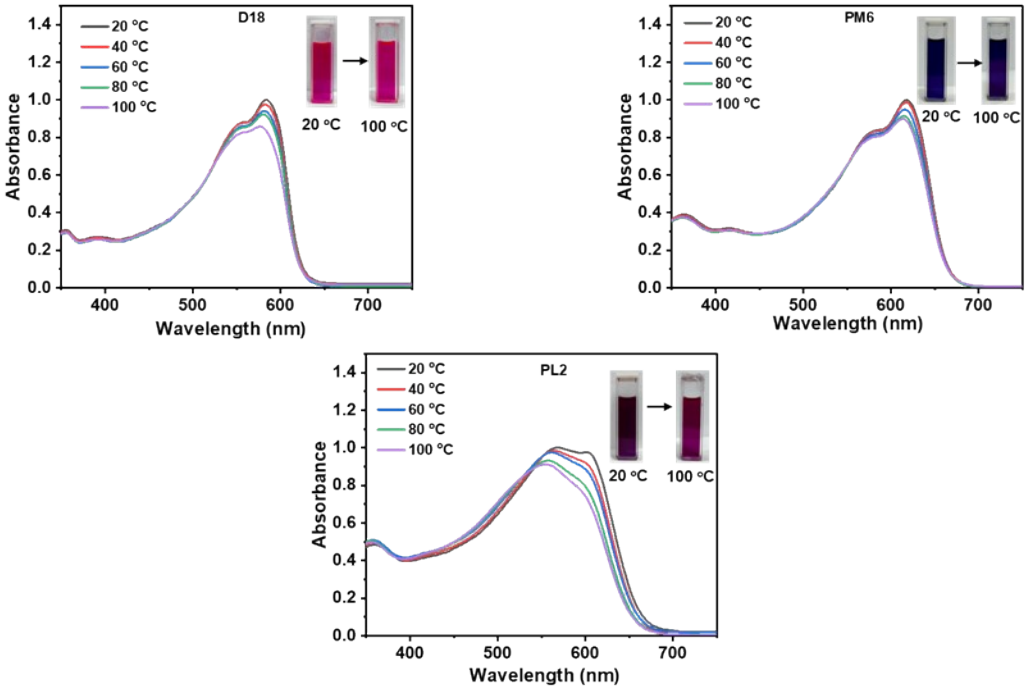

Figure S2. The UV–vis absorption spectra of D18, PM6 and PL2 at temperatures of 20–100 °C (The inset shows the solution under 20 and 100 °C, respectively).

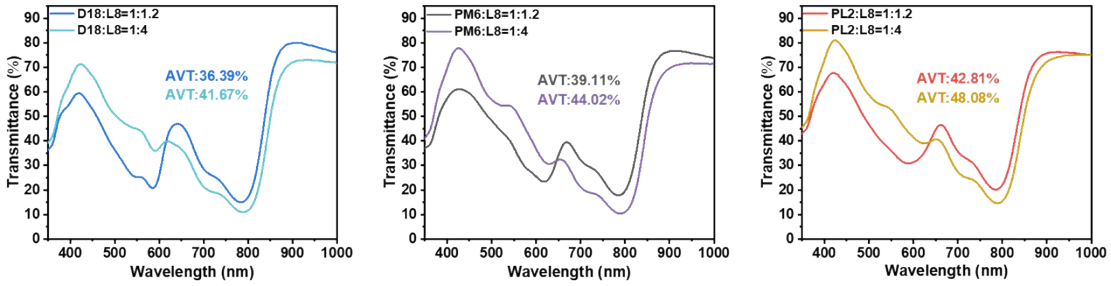

Figure S3. Transmittance of the active layer (D18:L8-BO, PM6:L8-BO, and PL2:L8-BO) before and after donor dilution.

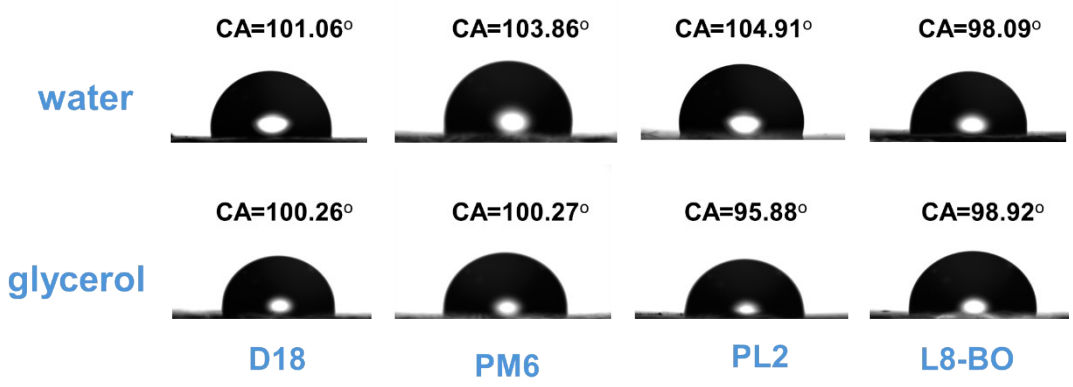

Figure S4. Contact angle photographs of water and glycerol droplets on pure D18, PM6, PL2 and L8-BO films.

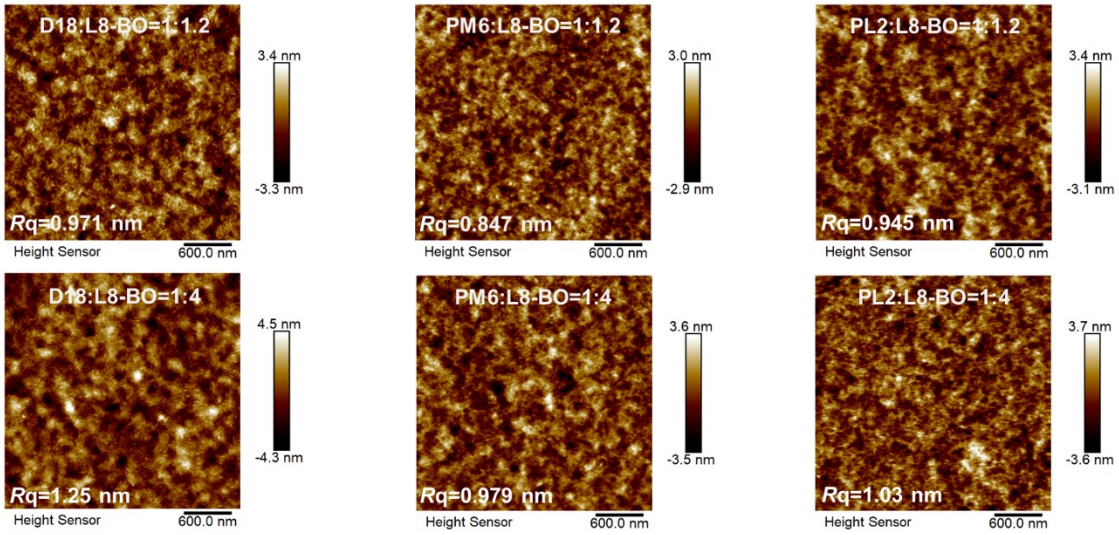

Figure S5. AFM height images of D18:L8-BO, PM6:L8-BO and PL2:L8-BO films with varying D:A ratios.

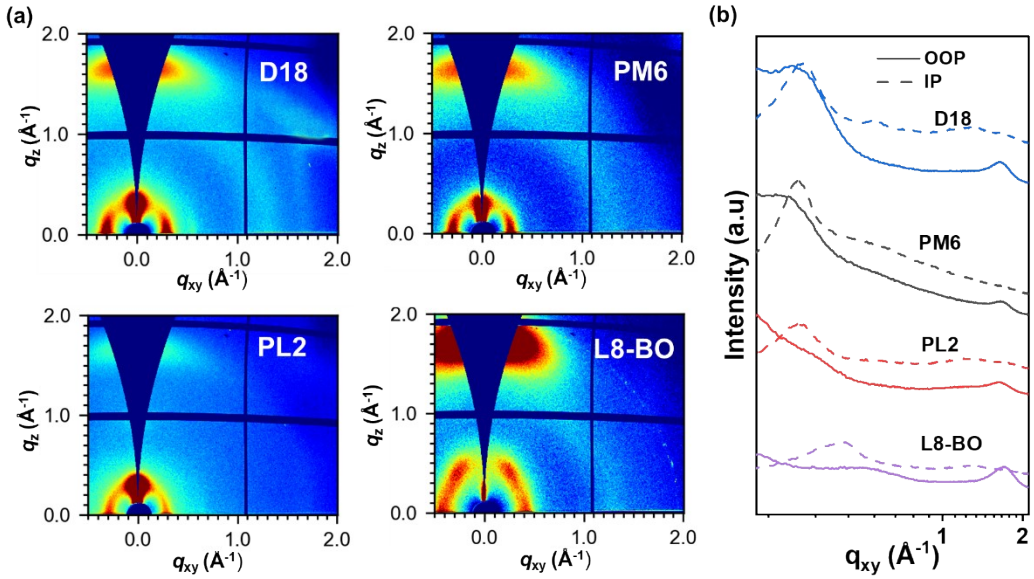

Figure S6. (a)The 2D GIWAXS patterns of neat film of D18, PM6, PL2 and L8-BO; (b) The GIWAXS 1D line-cuts of the in-plane (IP) and out-of-plane (OOP) directions.

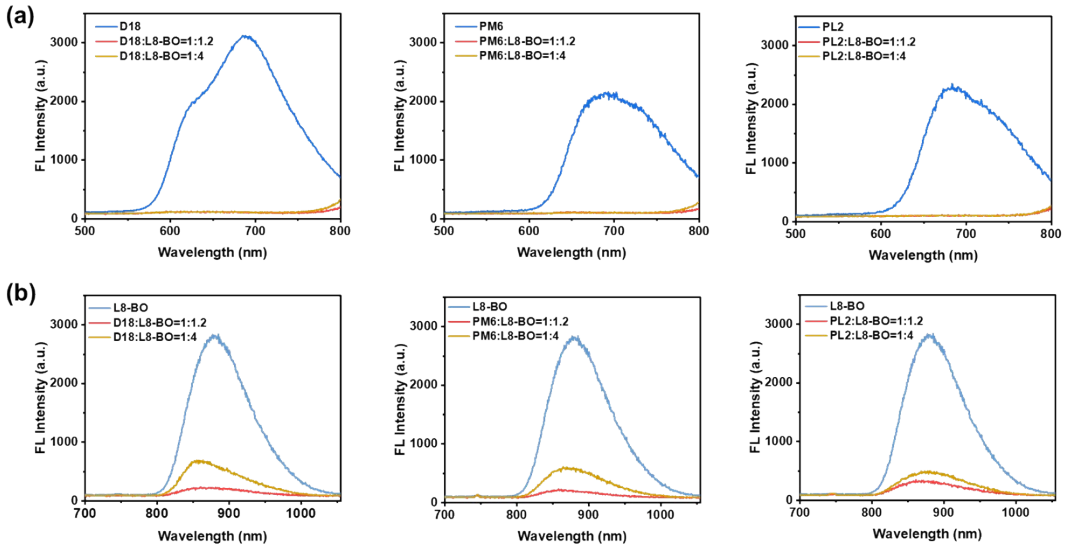

Figure S7. Photoluminescence spectra of neat and blend films: (a) Excitation at 500 nm (donor excitation); (b) Excitation at 750 nm (acceptor excitation).

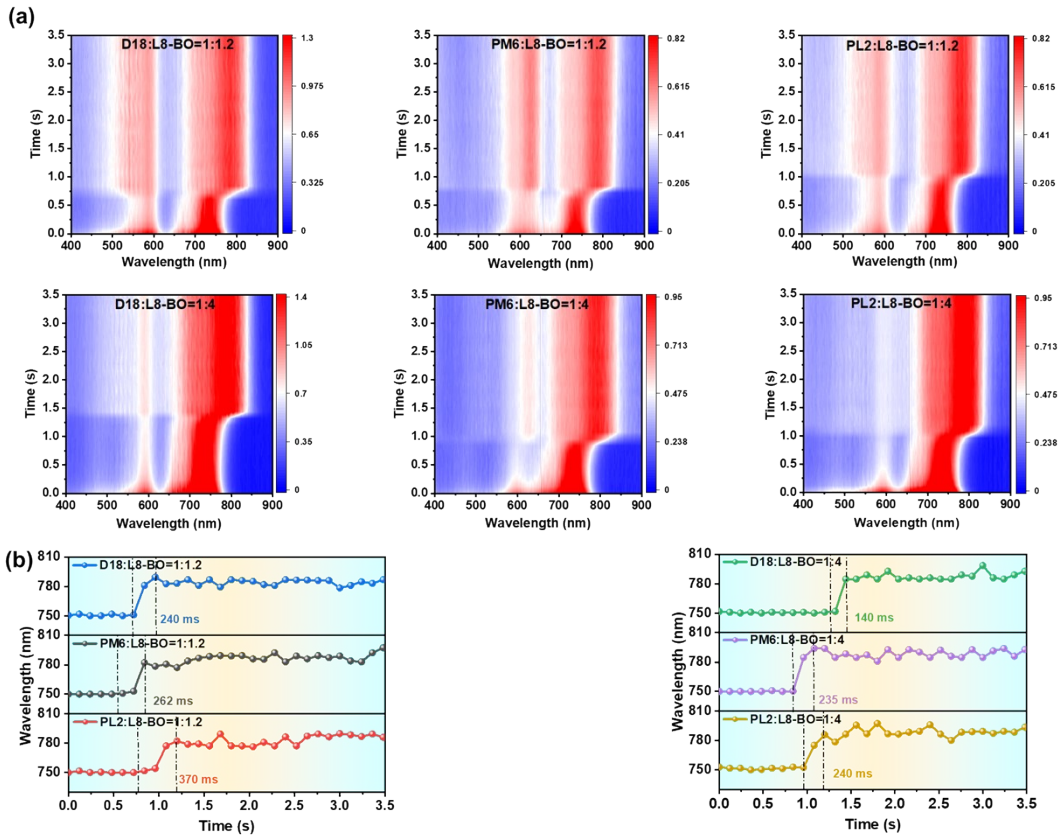

Figure S8. Time-dependent UV-vis absorption spectral evolution during spin-coating for three blend films at different D:A ratios: (a) Contour plot; (b) Corresponding time-integrated in situ absorption intensity of the acceptor.

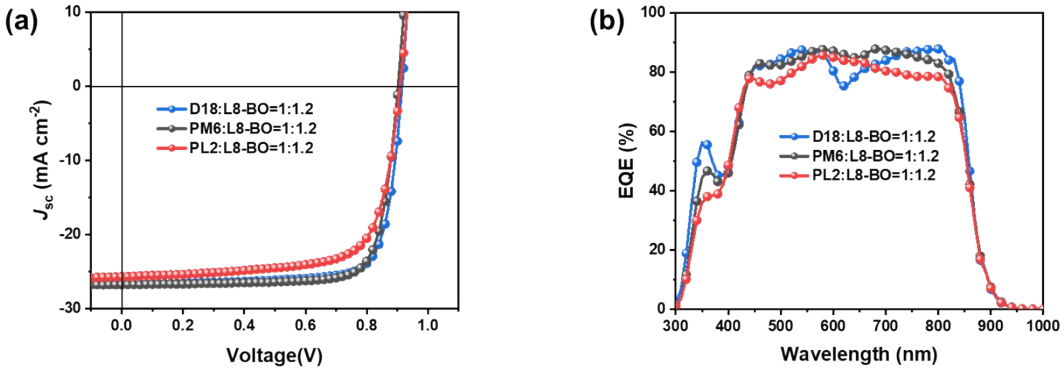

Figure S9. (a) *J-V* curves of devices; (b) The corresponding J_{sc} EQE spectra of the OSCs

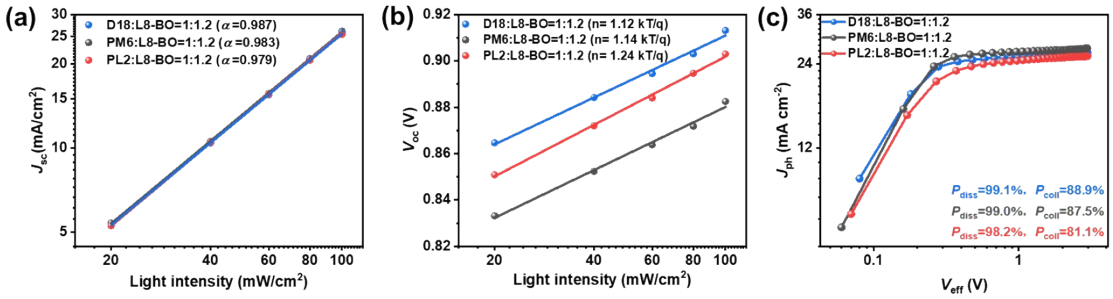

Figure S10. (a) J_{SC} versus light intensity, (b) V_{oc} versus light intensity, (c) J_{ph}-V_{eff} relationship of devices with D:A ratio of 1:1.2.

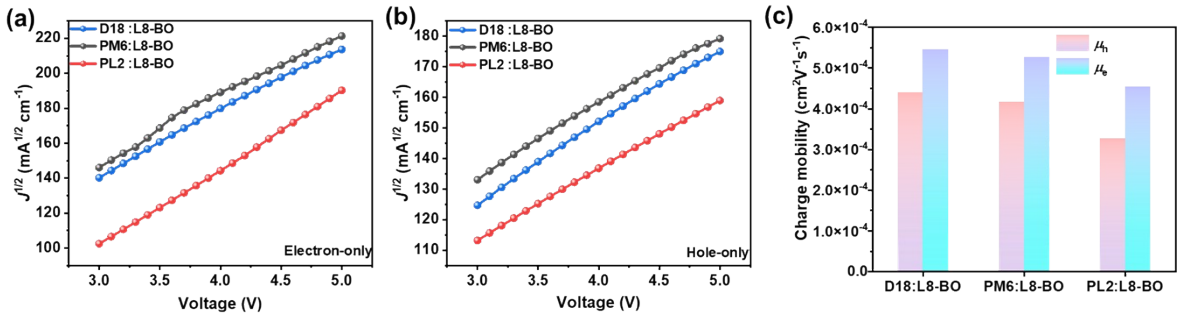

Figure S11. $J^{1/2}$-V characteristics of (a) electron-only and (b) hole-only devices with D:A ratio of 1:1.2, respectively; (c) corresponding hole and electron mobilities of different active layers.

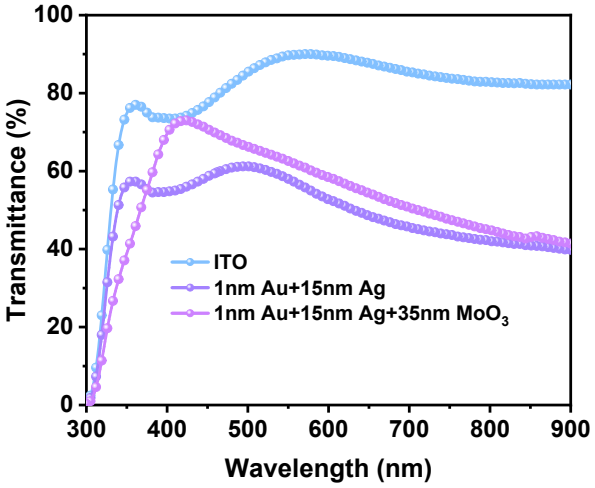

Figure S12. The transmittance of the electrodes used in the device

Table S1 Contact angles with water and glycerol and the calculated parameters.

Sample	θ_{water}(deg)	θ_{GL}(deg)	γ^d(mN m^{-1})	γ^p(mN m^{-1})	γ(mN m^{-1})	σ	Relative $X_{L8\text{-}BO:B}$ (K)[a]
D18	101.06	100.26	3.86	8.04	11.90	6.31	0.36
PM6	103.86	100.27	5.38	5.57	10.95	6.06	0.40
PL2	104.91	95.88	10.20	2.88	13.08	6.62	0.34
L8-BO	98.09	98.92	3.27	10.23	13.50	6.72	/

[a] B is D18, PM6 or PL2

Table S2 Summary of GIWAXS data in the OOP direction and of in the IP direction different neat films.

Peak position	Condition	q (Å^{-1})	d (Å)	FWHM (Å)	CCL (Å)
Out-of-plane (010)	D18	1.65	3.81	0.19	29.76
	PM6	1.64	3.83	0.20	28.27
	PL2	1.62	3.88	0.23	24.59
	L8-BO	1.69	3.72	0.27	20.94
In-plane (100)	D18	0.29	21.67	0.10	56.55
	PM6	0.30	20.94	0.08	70.68
	PL2	0.28	22.44	0.11	51.41
	L8-BO	0.42	14.96	0.20	28.27

Table S3 Summary of GIWAXS π-π stacking data in the OOP direction of different systems with various D/A weight ratios.

Peak position	Condition	q (Å^{-1})	d (Å)	FWHM (Å)	CCL (Å)
Out-of-plane (010)	D18:L8-BO=1:1.2	1.69	3.72	0.18	31.42
	PM6:L8-BO=1:1.2	1.68	3.74	0.20	28.27
	PL2:L8-BO=1:1.2	1.66	3.78	0.25	22.62
	D18:L8-BO=1:4	1.71	3.67	0.22	25.70
	PM6:L8-BO=1:4	1.69	3.71	0.23	24.59
	PL2:L8-BO=1:4	1.67	3.76	0.26	21.75

Table S4 Summary of GIWAXS lamellar stacking data in the IP direction of different systems with various D/A weight ratios.

Peak position	Condition	q (Å^{-1})	d (Å)	FWHM (Å)	CCL (Å)
In-plane (100)	D18:L8-BO=1:1.2	0.32	19.63	0.08	70.68
	PM6:L8-BO=1:1.2	0.31	20.27	0.09	62.83
	PL2:L8-BO=1:1.2	0.31	20.27	0.15	37.70
	D18:L8-BO=1:4	0.34	18.48	0.09	62.83
	PM6:L8-BO=1:4	0.32	19.63	0.11	51.41
	PL2:L8-BO=1:4	0.37	16.98	0.20	28.27

Table S5 Donor and Acceptor Fluorescence Quenching Efficiencies of D18:L8-BO, PM6:L8-BO, and PL2:L8-BO films at different ratios.

D:A	Active Layer	Donor Fluorescence Quenching Efficiency (%)	Acceptor Fluorescence Quenching Efficiency (%)
1:1.2	D18:L8-BO	100	91.7
	PM6:L8-BO	99.9	91.8
	PL2:L8-BO	99.9	88.1
1:4	D18:L8-BO	100	75.6
	PM6:L8-BO	100	78.4
	PL2:L8-BO	100	82.4

Table S6 Photovoltaic and transparency performances of OSCs with different PL2:L8-BO ratios under the illumination of AM 1.5G.

D:A	V_{OC}[V]	J_{SC}[mA cm^{-2}]	FF[%]	PCE (%)	Film AVT (%)	Film LUE (%)
1:1.2	0.908	25.69	72.09	16.80 (16.75 ± 0.08)	42.81	7.19
1:2	0.912	25.16	71.10	16.31 (16.28 ± 0.06)	44.16	7.20
1:3	0.913	23.77	71.99	15.62 (15.55 ± 0.10)	45.63	7.13
1:4	0.911	23.23	71.72	15.16 (15.04 ± 0.12)	48.08	7.29
1:5	0.912	22.89	65.72	13.72 (13.60 ± 0.12)	52.59	7.21

Table S7 SCLC-derived electron/hole mobility for D18:L8-BO, PM6:L8-BO, and PL2:L8-BO blend films with D:A ratio of 1:1.2 and 1:4

D:A	Blend film	μ_e [10^{-4} cm^2 $V^{-1}s^{-1}$]	μ_h [10^{-4} cm^2 $V^{-1}s^{-1}$]	μ_e/μ_h
1:1.2	D18:L8-BO	5.45	4.39	1.24
	PM6:L8-BO	5.27	4.16	1.26
	PL2:L8-BO	4.55	3.26	1.39
1:4	D18:L8-BO	6.08	1.85	3.29
	PM6:L8-BO	6.25	2.14	2.91
	PL2:L8-BO	6.34	2.62	2.42

References

1. K. Jin, Z. Xiao and L. Ding, *J. Semicond.,* 2021, **42**, 060502.
2. H. Lu, H. Wang, G. Ran, S. Li, J. Zhang, Y. Liu, W. Zhang, X. Xu and Z. Bo, *Adv. Funct. Mater.,* 2022, **32**, 2203193.
3. J. Yao, S. Ding, R. Zhang, Y. Bai, Q. Zhou, L. Meng, E. Solano, J. A. Steele, M. B. J. Roeffaers, F. Gao, Z.-G. Zhang and Y. Li, *Adv. Mater.,* 2022, **34**, 2203690.
4. J. Yao, B. Qiu, Z.-G. Zhang, L. Xue, R. Wang, C. Zhang, S. Chen, Q. Zhou, C. Sun, C. Yang, M. Xiao, L. Meng and Y. Li, *Nat. Commun.,* 2020, **11**, 2726.
5. J. Comyn, *Int. J. Adhes. Adhes.,* 1992, **12**, 145-149.
6. S. Nilsson, A. Bernasik, A. Budkowski and E. Moons, *Macromolecules,* 2007, **40**,

8291-8301.